Thermal oxidation kinetics of additive free polyamide 6-6

C. El-Mazry [a,b], M. Ben Hassine [b], O. Correc [a], X. Colin [b,*]

[a] CSTB, Aquasim, 11 rue Henri Picherit, 44300 Nantes Cedex, France
[b] Arts et Metiers ParisTech, Laboratoire PIMM, 151 boulevard de l'Hôpital, 75013 Paris, France

A B S T R A C T

Thermal aging of an additive free PA 6-6 has been elucidated at 90, 100, 120, 140, 150 and 160 °C in air-ventiled ovens by Fourier transform infrared spectrophotometry, viscosimetry in molten state and uniaxial tensile testing. Oxidation of methylene groups starts after a considerably shorter induction period but reaches a lower maximal rate than in additive free PE. Cleavage of C—N bonds constitutes the main source of chain scissions. It leads to the formation of aldehyde chain-ends and a catastrophic decrease in molar mass. Embrittlement occurs at a very low conversion ratio of the oxidation process, in particular when the concentration of aldehyde chain-ends reaches a critical value of $[PH{=}O]_F \approx 5.6\ 10^{-3}$ mol l^{-1}, corresponding to a critical value of the number average molar mass of $M_{nF} \approx 17$ kg mol^{-1}. At this stage, the entanglement network in the amorphous phase is deeply damaged.

A non-empirical kinetic model has been derived from the oxidation mechanistic scheme previously established for PE, but improved by adding elementary reactions specific to polyamides such as the rapid decomposition of unstable hydroxylated amide groups. This model describes satisfyingly the main features of the thermal oxidation kinetics of PA 6-6, but also of other types of aliphatic polyamides studied previously in the literature such as: PA 6, PA 12 and PA 4-6, as long as it is not controlled by oxygen diffusion. At the same time, it confirms the existence of an universal character for the thermal oxidation kinetics of aliphatic polyamides whatever their origin, i.e. their initial molar mass, crystallinity ratio, concentration of impurities, structural irregularities, etc.

Keywords:
Aliphatic polyamides
Thermal oxidation
Chain scission
Embrittlement
Kinetic modeling

1. Introduction

Polyamides (PAs) are increasingly considered for technical applications because of their excellent resistance to mechanical fatigue, friction and many chemical substances (e.g. oils, greases and hydrocarbons), but also their high barrier properties to liquids and gases. They have already found many applications in various industrial sectors such as offshore (e.g. pipes for the transport of oil and natural gas), automotive (e.g. radiators for the cooling of motors) or drinking water distribution (e.g. safety parts in domestic networks). In most cases, PA pieces are exposed in aggressive environments, where they are in contact with chemical reagents such as water, oxygen, chlorine disinfectants, etc., which poses the problem of their long term durability.

Since the late 1950s, many research works have been devoted to hydrolytic aging of PAs e.g. [1—9]. This type of chemical aging is now fairly well understood [10]. Recently, a heuristic kinetic model has been derived from the classical mechanistic scheme for reversible hydrolysis in order to access to the molecular and macromolecular changes (against time of exposure), but also to the consequences of these changes on morphology and fracture properties [10]. Now, a new challenge is to determine and elucidate the relationships between PAs structure and rate constants of hydrolysis and condensation reactions by using the kinetic model as an inverse method.

On the contrary, too few research works have been devoted to the thermal aging of additive free PAs [8—29] and their model compounds [14,16,20,21,29,30] to be able to define, at the present time, a general approach for lifetime prediction. Moreover, these studies have focused only on certain aliphatic PAs: essentially PA 6 [11—25] and PA 6-6 [8,9,11,12,26—29], but rarely PA 12 [13,15,16] and PA 4-6 [15,28]. Finally, their thermal oxidation mechanisms and kinetics have been investigated by a small number of analytical techniques, in particular: oxygen absorption [8,14—17,20,21,25,28,30], Fourier transform infra-red (FTIR) [17,22,25] and visible/ultra-violet spectrophotometries (Vis—UV) [11,12,16,25,27], nuclear magnetic resonance spectroscopy (NMR) [16], chemical titration [14—17,23,25,27,30], chemiluminescence (CL) [13,15—18,20—22,25,26,29,30] and differential calorimetry under pure oxygen (TIO) [17,19,22].

* Corresponding author. Tel.: +33 1 44 24 61 47; fax: +33 1 44 24 63 82.
E-mail address: xavier.colin@ensam.eu (X. Colin).

Nevertheless, from the oxidation kinetic curves obtained by plotting the chemical property under consideration versus time of exposure, two important kinetic quantities can be determined graphically (Fig. 1):

- Induction time (t_i) would correspond to the period of time during which the effects of oxidation are too small to be detected by common laboratory analytical techniques.
- Maximal oxidation rate (r_S) would correspond to the steady-state oxidation rate if the substrate concentration has not been excessively reduced by the rapid auto-acceleration of oxidation at the end of the induction period [31].

Values of t_i and r_S of additive free PAs have been tentatively compiled between 100 and 200 °C from the literature of the past half century [11,13–23,25–30]. Unfortunately, t_i was too short to be correctly estimated, even from real-time analysis techniques such as oxygen absorption, differential calorimetry (TIO) or chemiluminescence (CL). As a result, only values of r_S deserved to be exploited. As an example, values of r_S determined in air or pure oxygen (under atmospheric pressure) are reported in the Arrhenius diagram of Fig. 2. These values are compared to those determined for another important type of polymethylenic substrate extensively studied in the literature and thus, selected as a reference material in this study: additive free polyethylene (PE) [32,33].

From a kinetic analysis of these experimental data, it is possible to get an idea of the resistance to thermal oxidation of aliphatic PAs compared to PE, but also to highlight the main peculiarities of their oxidation kinetics. In the temperature range under study, one can see that:

- The oxidation kinetics of both types of polymethylenic substrates exhibits an universal character whatever their origin, i.e. their initial molar mass, crystallinity ratio, degree of branching, concentration of impurities, structural irregularities, etc.
- r_S obeys an Arrhenius law with a different pre-exponential factor, but almost the same activation energy for both types of polymethylenic substrates (Table 1), which would suggest that there are similarities between their thermal oxidation mechanisms and kinetics.
- Oxidation of methylene groups starts from the early periods of exposure in aliphatic PAs, whereas it starts after a well-marked induction period in PE. In contrast, the maximal oxidation rate is significantly lower (about 20–100 times lower) in aliphatic PAs than in PE.

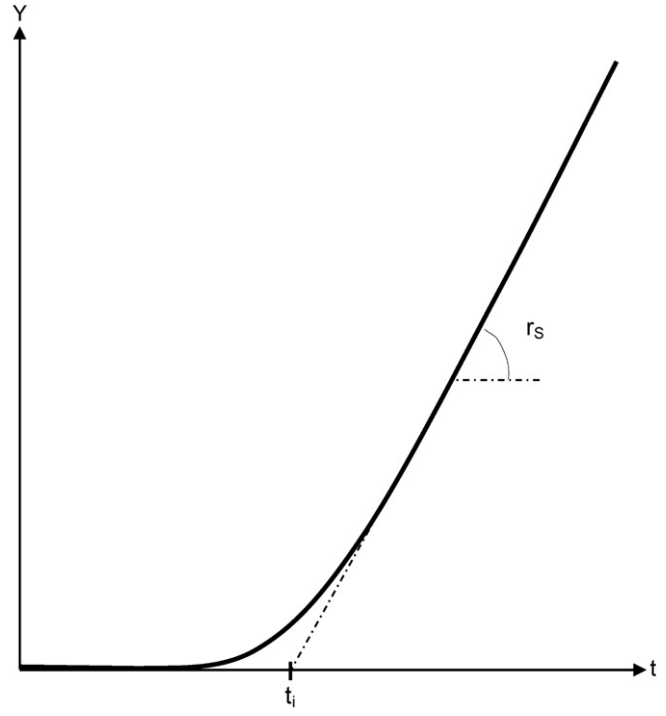

Fig. 1. General shape of oxidation kinetic curves. Y designates a chemical quantity changing during thermal aging of hydrocarbon polymers. Graphical determination of induction time (t_i) and maximal oxidation rate (r_S).

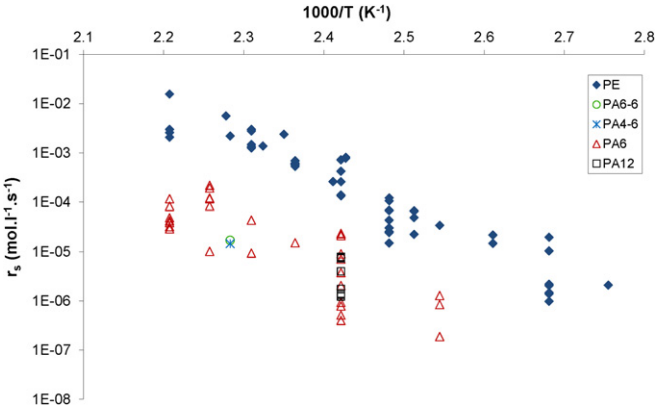

Fig. 2. Arrhenius plot of the maximal oxidation rate (r_S) of additive free aliphatic PAs and PE in air or pure oxygen (under atmospheric pressure) between 90 and 200 °C.

Such differences can be tentatively explained by using, in a first approach, relatively simple kinetic equations derived from the classical version of the standard oxidation scheme at low to moderate temperatures (typically for $T < 200$ °C) in oxygen excess [34]. In such thermal aging conditions, oxidation is essentially initiated by the bimolecular decomposition of hydroperoxide groups (POOH) [35]. Then, t_i and r_S can be expressed by [35]:

$$t_i = \frac{1 - \ln Y_0}{\sqrt{2 r_S k_{1b}}} \quad \text{with} \quad Y_0 = \frac{[\text{POOH}]_0}{[\text{POOH}]_S} \tag{1}$$

$$r_S = \frac{k_3^2 [PH]^2}{2 k_{6\ \text{app}}} \tag{2}$$

where k_{1b}, k_3 and $k_{6\ \text{app}}$ are initiation, propagation and apparent termination rate constants respectively. $[\text{POOH}]_0$ and $[\text{POOH}]_S$ are initial and steady-state concentrations of POOH respectively. [PH] is the concentration of oxidizable CH groups in the amorphous phase. Examples of [PH] values for aliphatic PAs and PE have been reported in Table 2.

According to these equations, only a combination of high values of k_{1b} and $k_{6\ \text{app}}$ would allow to obtain simultaneously low values of t_i and r_S. This important result can be interpreted as follows: Hydroperoxide groups (POOH) would be more unstable and

Table 1
Arrhenius parameters: pre-exponential factor (r_{S0}) and activation energy (E_S), for maximal oxidation rate (r_S) of additive free aliphatic PAs and PE in oxygen excess between 90 and 200 °C.

Polymers	r_{S0} (l mol^{-1} s^{-1})	E_S (kJ mol^{-1})
PE	5.5×10^{13}	138
PAs	1.4×10^{9}	115

Table 2
Physico-chemical characteristics of some aliphatic PAs and PE [36,37]: molar mass of monomer unit (m_{UCR}), density of amorphous phase (ρ_a), concentration of oxidizable groups in the amorphous phase [PH], average values of density (ρ) and crystallinity ratio (X_C).

Polymer	m_{UCR} (kg mol^{-1})	ρ_a	[PH] (mol.l^{-1})	ρ	X_C (%)
PA 6-6	226	1.08	9.6	1.14	50
PA 4-6	198	1.08	10.9	1.18	70
PA 6	113	1.08	9.6	1.13	50
PA 12	197	0.99	5.5	1.02	35
PE	28	0.85	60	0.94	50

secondary peroxy radicals ($PO_2^{\cdot}$) would be more reactive in aliphatic PAs than in PE.

The aim of the present article is double. First of all, it is to outline the main characteristics of a non-empirical kinetic model predicting the thermal oxidation of additive free aliphatic PAs, and to check its validity for PA 6-6. Because of the existence of striking similarities between the oxidation kinetics of additive free aliphatic PAs and PE, this model will be derived from the oxidation mechanistic scheme previously established for PE [38], but improved by adding elementary reactions specific to PAs of which the key importance has been clearly evidenced by several authors in the literature [11,28,39–42]. Secondly, it is to use this sophisticated numerical tool for interpreting experimental results published previously in the literature, in particular for explaining the main differences and similarities between the thermal oxidative behaviors of both polymethylenic substrates and elucidating the universal character of the oxidation kinetics of aliphatic PAs.

2. Experimental

2.1. Material

Unstabilized and unfilled PA 6-6 pellets were supplied by Rhodia. Their main characteristics are: glass transition temperature: $T_{g0} = 38.6 \pm 4.5$ °C, melting point $T_{m0} = 266.9 \pm 1.2$ °C, crystallinity ratio $X_{C0} = 42 \pm 2\%$, density $\rho_0 = 1.14$ kg m^{-3}, weight average molar mass $M_{W0} = 37.3$ kg mol^{-1} and molar mass distribution $IP_0 \approx 2$.

Prior to processing, pellets were carefully dried at 80 °C during 72 h under a primary vacuum in order to prevent hydrolysis at high temperature in molten state. Then, thin PA 6-6 films, with thicknesses ranging from 30 to 100 μm, were elaborated by compression molding at 270 °C under a pressure of 17 MPa. They were kept in a desiccator containing silica-gel in order to prevent any moisture uptake before oxygen permeation and thermal aging tests.

2.2. Ageing conditions and methods of characterization

2.2.1. Oxygen permeation

Oxygen transport properties in PA 6-6 were determined at 23, 30 and 40 °C by permeation. Although it is considered less sensitive than gravimetric, barometric or volumetric sorption methods [43], permeation was chosen for this study because it is, still today, the most widely used method for the determination of transport properties of gases in polymers, in particular in the field of packaging where it has been the subject of international standards [44,45]. That is presumably the reason why values of oxygen solubility and diffusivity, compiled from the literature of the past half century and reported in reference books in this area [46] and in polymer handbooks [47,48], were almost all determined by this method. Due to a large amount of analytical data, permeation appeared to us as an interesting tool for the elucidation of structure/oxygen transport property relationships in polymers.

A thin PA 6-6 film was placed between the two compartments of a Systech 8001 permeameter: the upstream compartment was maintained under a pure oxygen pressure of 2–3 bars, whereas the downstream one was swept by an oxygen free gas carrier (in this case, pure nitrogen) under atmospheric pressure. The pressure difference induced an oxygen flow through the sample thickness. The cumulative oxygen flow Q in the downstream compartment was determined by a coulometric detector. Its general shape versus time of exposure is presented in Fig. 3.

Two important kinetic quantities were determined graphically:

- Time lag (t_L) would correspond to the duration of the transient regime. It is the characteristic time for oxygen diffusion through a polymer membrane of thickness L. According to Barrer [49], t_L is inversely proportional to the coefficient of oxygen diffusion D_{O_2}:

$$t_L = \frac{L^2}{6\,D_{O_2}} \tag{3}$$

- Oxygen permeability (P_e) would correspond to the slope of the steady-state straight-line. Its general expression is:

$$P_e = S_{O_2} \times D_{O_2} \tag{4}$$

where S_{O_2} is the coefficient of oxygen solubility.

Coefficients D_{O_2} and S_{O_2} were calculated at each temperature under study from Eqn. (3) and (4). Then, the equilibrium oxygen concentration [O_2] was deduced by using the classical Henry's law:

$$[O_2] = S_{O_2} \times p_{O_2} \tag{5}$$

where p_{O_2} is the oxygen partial pressure in the aging environment. As an example, in air under atmospheric pressure, $p_{O_2} = 0.21$ bar.

It was found that D_{O_2} obeys an Arrhenius law for PA 6-6 in glassy state. As an indication, its corresponding Arrhenius parameters are reported in Table 3.

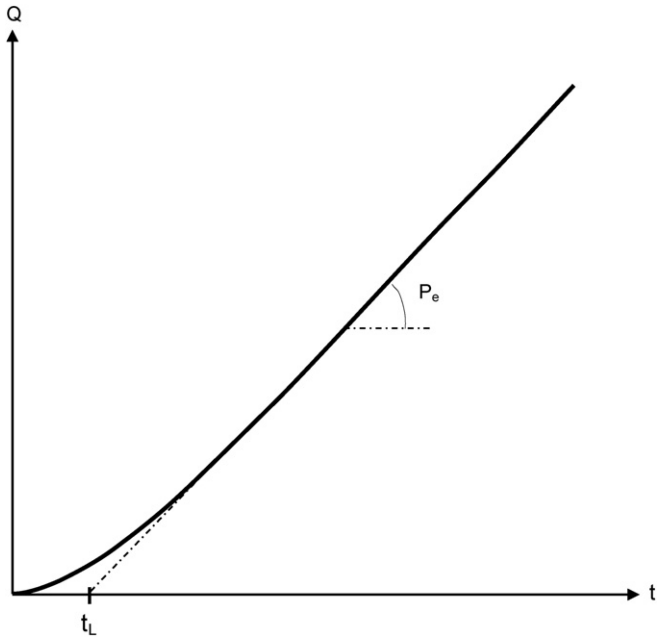

Fig. 3. General shape of the cumulative oxygen flow versus exposure time in the downstream compartment of a permeameter. Graphical determination of time lag (t_L) and oxygen permeability (P_e).

Table 3
Arrhenius parameters: pre-exponential factor (P_0) and activation energy (E_a), for coefficients of oxygen diffusion (D_{O_2}) and solubility (S_{O_2}) of PA 6-6 between 23 and 40 °C.

	P_0	E_a (kJ mol^{-1})
D_{O_2} (m^2 s^{-1})	4.7×10^{-4}	52.8
S_{O_2} (mol l^{-1} Pa^{-1})	1.7×10^{-8}	0

On the contrary, S_{O_2} varies erratically with temperature confirming that, in PA 6-6 as in almost all other polymers [50], it is practically temperature independent. Between 23 and 40 °C, its average value is:

$$S_{O_2} = (1.7 \pm 0.5) \times 10^{-8} \text{ mol l}^{-1} \text{ Pa}^{-1}$$

i.e. $(3.8 \pm 1.1) \times 10^{-2}$ cm^3(STP) cm^{-3} bar^{-1}

It leads to an average value of equilibrium oxygen concentration in air of:

$$[O_2] = 3.6 \times 10^{-4} \text{ mol l}^{-1}$$

i.e. 8.0×10^{-3} cm^3(STP) cm^{-3}

In a first approach, such average values have been kept for modeling the thermal oxidation kinetics of PA 6-6 between 90 and 160 °C, although discontinuities may appear in the Arrhenius graphs of oxygen transport properties [51]. This choice results essentially from the fact that it is impossible to perform oxygen permeation tests without oxidizing additive free PA 6-6 films above 90 °C and thus, to determine non-erroneous values of S_{O_2}.

2.2.2. Thermal aging tests

PA 6-6 films were exposed in air-circulating ovens 90, 100, 120, 140, 150 and 160 °C during several hundreds of hours. Films were regularly removed from the ovens and stored at room temperature in a desiccator containing silica-gel in order to avoid moisture absorption before characterization. The films were characterized by conventional laboratory techniques in order to determine the resulting structural changes at different pertinent scales (i.e. molecular, macromolecular and macroscopic scales).

2.2.3. FTIR spectrophotometry

After thermal aging, PA 6-6 films were first analyzed by Fourier transform IR spectrophotometry (Brüker IFS 28 spectrometer, minimal resolution of 4 cm^{-1}) between 400 and 4000 cm^{-1} in a transmission mode. As previously evidenced by Gonçalves et al. [42], two main molecular changes were clearly put in evidence on FTIR spectra (Fig. 4):

- Between 3000 and 3150 cm^{-1}, one observes the progressive disappearance of the peak centered at 3080 cm^{-1}. According to Cannon [52], this peak is the result of two different contributions: Stretching of C–N bonds and deformation of N–H bonds. Stretching of C–N bonds is by far the main contribution at low conversion ratio of oxidation process [42]. Indeed, by making a mathematical deconvolution (Fig. 5), deformation of N–H bonds can be revealed as a small shoulder centered at 3060 cm^{-1}. Since amide groups (CO–NH) are stable during PA 6-6 oxidation at moderate to low temperatures (typically for T < 200 °C), the progressive disappearance of the peak centered at 3080 cm^{-1} has been obviously attributed to the cleavage of the C–N bonds of amino-aliphatic type ($NH-CH_2$), i.e. to the transformation of monosubstituted amide groups ($CO-NH-CH_2$) into non-substituted ones ($CO-NH_2$) [42].
- Between 1670 and 1810 cm^{-1}, one observes the progressive appearance and increase of a series of carbonyl peaks. The most intense peak is centered at 1735 cm^{-1}.

On the contrary, no change in absorbance was detected in the hydroxyl region (i.e. typically between 3300 and 3650 cm^{-1}), indicating that there is no formation of stable hydroxylated products (in particular alcohols and carboxylic acids) during PA 6-6 thermal oxidation (Fig. 4). That is the reason why, in a first approach, it was assumed that the new carbonyl species are mainly composed of aldehyde chain-ends (PH=O).

The absorbances of the peaks relative to C–N bonds and PH=O chain-ends were determined after mathematical deconvolution of the absorption bands overlapped respectively between 3000 and 3150 cm^{-1} and 1670 and 1810 cm^{-1}. Examples of deconvolution, made before thermal aging, are reported in Fig. 5.

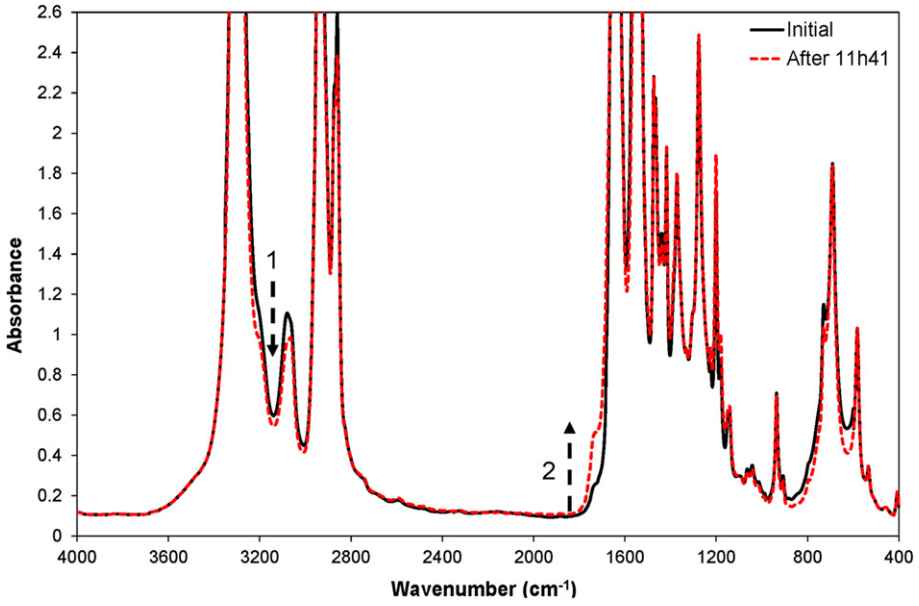

Fig. 4. FTIR spectrum of a PA 6-6 film of about 30 μm thick before and after 11 h 45 min of thermal aging at 150 °C in air.

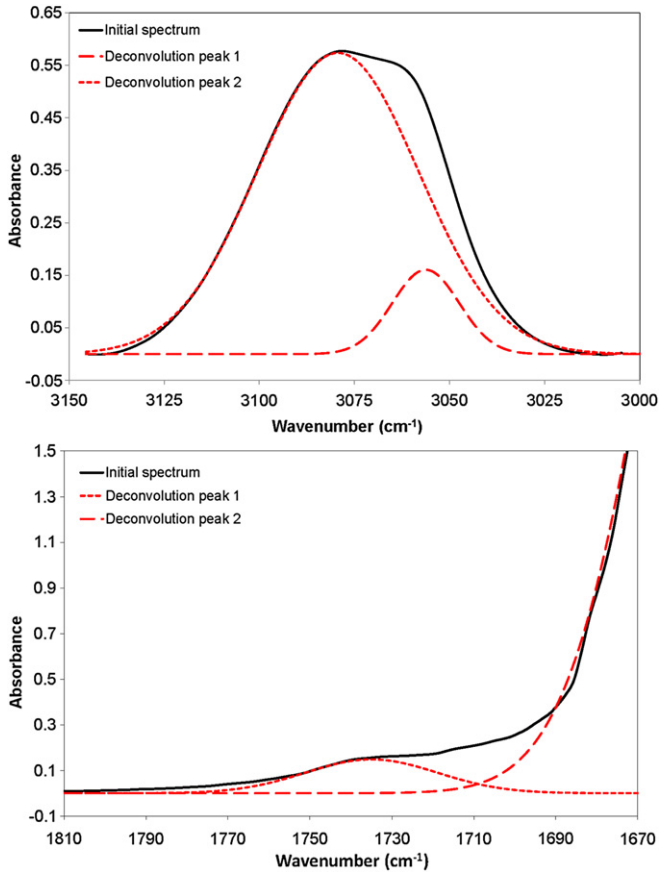

Fig. 5. Mathematical deconvolution of the absorption bands overlapped in the FTIR spectra of a virgin PA 6-6 film (see Fig. 5). Top: Between 3000 and 3150 cm^{-1} before thermal aging. Bottom: Between 1670 and 1810 cm^{-1}.

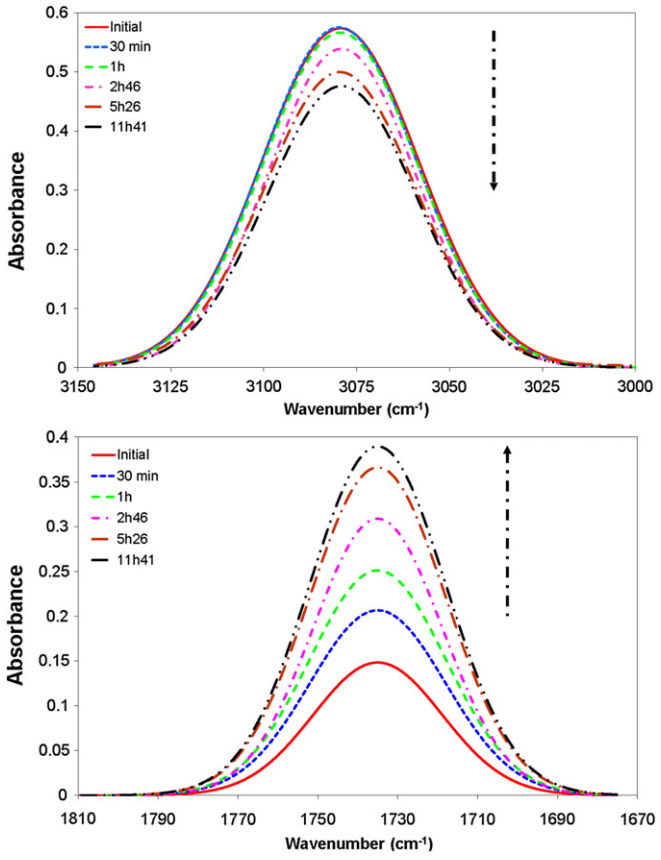

Fig. 6. Peaks resulting from the deconvolution of the FTIR spectra of PA 6-6 films before and after thermal aging at 150 °C in air (see Fig. 6). Top: Peak relative to C–N bonds at 3080 cm^{-1}. Bottom: Peak relative to PH=O chain-ends at 1735 cm^{-1}.

The changes in absorbance against time of exposure at 150 °C in air of both IR peaks are reported in Fig. 6.

Then, the concentrations of C–N bonds and PH=O chain-ends were determined by using the classical Beer–Lambert's law:

$$\mathrm{Abs}(Y) = \varepsilon_Y L[Y] \tag{6}$$

where Abs(Y), ε_Y and $[Y]$ are respectively the absorbance, the coefficient of molar absorptivity and the concentration of the chemical specie Y under consideration for a polymer film of thickness L.

Coefficient ε_{C-N} was determined for a series of virgin PA 6-6 films, with thicknesses ranging from 30 to 100 μm, knowing that initial concentrations of C–N bonds in the amorphous phase are: $[CO-NH]_0=[NH-CH_2]_0 \approx 9.6$ mol l^{-1}. It was found that: $\varepsilon_{C-N} \approx 45$ l mol^{-1} cm^{-1}. In contrast, value of $\varepsilon_{PH=O}$ was found in the literature: $\varepsilon_{PH=O} = 200$ l mol^{-1} cm^{-1} [13].

2.2.4. Rheometry

Afterwards, PA 6-6 films were analyzed by viscosimetry (TA Instruments ARES rheometer) under nitrogen in molten state, at 265 °C, using a coaxial parallel plate geometry, a plate diameter of 25 mm and a gap of 1 mm, in order to evaluate the macromolecular changes. Sweep angular frequency experiments were performed in a relatively large frequency domain (typically between 0.1 and 100 $rad.s^{-1}$) with a strain amplitude of 5%. These experiments show that the PA 6-6 rheological behavior is Newtonian in the low frequency range, typically for $\omega \leq 30$ rad s^{-1}. Moreover, as expected in the case of a predominant chain scission process, the Newtonian plateau is a decreasing function of exposure time (Fig. 7).

Thus, the decreases in weight average molar weight M_W were determined from the decreases in Newtonian viscosity η using the classical Bueche's equation [53,54]:

$$\eta = K\ M_W^{3.4} \tag{7}$$

where K is a constant depending only on molecular structure and temperature.

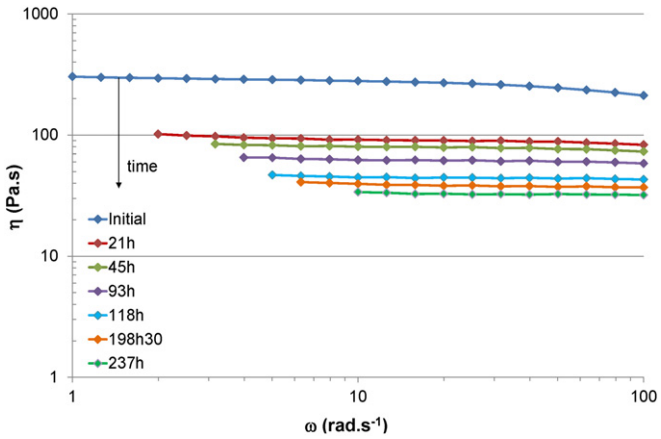

Fig. 7. Curves of dynamic melt viscosity versus angular frequency at 265 °C for PA 6-6 before and after thermal aging at 100 °C in air.

K was determined at 265 °C from the initial values of the weight average molar mass $M_{W0} = 37.3$ kg mol^{-1} and Newtonian viscosity $\eta_0 = 350 \pm 40$ Pa s of PA 6-6 films:

$$K = \frac{\eta_0}{M_{W0}^{3.4}} = 1.6 \times 10^{-3} \text{Pa (kg mol)}^{-3.4} \quad (8)$$

In the case of a predominant chain scission process, the polydispersity index IP will not change during exposure: IP = IP$_0$ = 2, so that:

$$M_n = M_W/2 \quad (9)$$

2.2.5. Uniaxial tensile testing

At least, PA 6-6 films were characterized by uniaxial tensile testing (Instron 4310 machine) at 23 °C and 50% RH, with a strain rate of 7.5 × 10^{-3} s^{-1}, in order to evaluate the consequences of macromolecular changes on the mechanical behavior. It was observed that the main changes on tensile curves take place in the early periods of thermal exposure. They consist in the disappearance of the plastic plateau (Fig. 8). Thus, the initially semi-ductile PA 6-6 becomes rapidly brittle and, from that moment, its failure occurs in the absence of necking. That is the reason why, in this study, a peculiar attention was paid on the ultimate elongation ε_R in order to determine a structural endlife criterion for PA 6-6.

3. Theoretical

3.1. Mechanistic scheme

Aliphatic PAs are constituted of polymethylenic sequences. As an example, the chemical structure of PA 6-6 is:

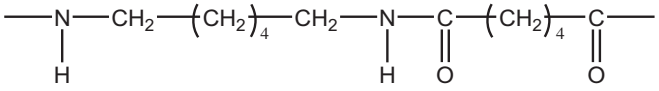

It is thus expected that such polymers family oxidizes according to a mechanistic scheme very close to that previously established for another important type of polymethylenic substrate: PE [38]. According to this mechanism, oxidation propagates both by incorporation of oxygen and abstraction of labile hydrogen atoms:

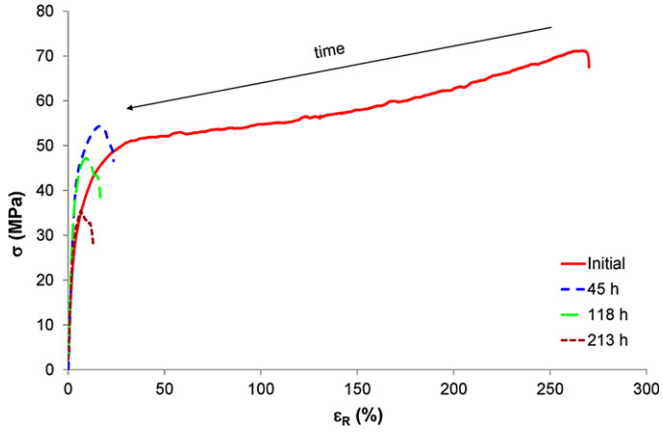

Fig. 8. Tensile curves of PA 6-6 films of about 100 μm thick before and after thermal aging a 100 °C in air.

Table 4
Arrhenius parameters and orders of magnitude at 30 °C of rate constant k_3 for common methylenic C–H bonds [35,58,59]. Notations: PE: polyethylene; PA: polyamide; PET: poly(ethylene terephthalate); PBT: poly(butylene terephthalate); PBD: polybutadiene.

Methylenic C–H bond	k_{30} (l mol^{-1} s^{-1})	E_3 (kJ mol^{-1})	k_{30} at 30 °C (l mol^{-1} s^{-1})	Polymers
–CH$_2$–CH$_2$–	1.5 × 10^{10}	73	4.0 × 10^{-3}	PE
>N–CH$_2$– or –O–CH$_2$–	1.8 × 10^{9}	63	2.5 × 10^{-2}	PAs, PET, PBT
–CH=CH–CH$_2$–	4.0 × 10^{9}	68	7.7 × 10^{-3}	PBD

$$P^{\cdot} + O_2 \rightarrow PO_2^{\cdot} \quad (k2)$$

$$PO_2^{\cdot} + PH \rightarrow POOH + P^{\cdot} \quad (k3)$$

where P$^{\bullet}$, PO$_2^{\bullet}$, PH and POOH designate respectively alkyl and peroxy radicals, polymer substrate and hydroperoxides. k_2 and k_3 are the corresponding rate constants.

Of course, the first step is very fast and practically temperature and structure independent: $k_2 = 10^8$–10^9 l mol s^{-1} [55]. At the opposite, the second step is considerably slower: it is even slower than the dissociation energy E_D of the C–H bond is higher. Structure/k_3 relationships have been investigated by Korcek et al. [56]. According to these authors, Log(k_3) would be a linear function of E_D. Thus, in PA 6-6, it would be necessary to distinguish two types of methylenic C–H bonds:

- Those belonging to tetramethylenic sequences for which $E_D \approx 393$ kJ mol^{-1}.
- From those located in α position of the (electronegative) nitrogen atoms for which E_D is noticeably lower: $E_D \approx 376$ kJ mol^{-1}.

As a piece of information, the Arrhenius parameters and orders of magnitude at 30 °C of the rate constant k_3 for common methylenic C–H bonds are reported in Table 4. These values have been compiled from previous research works performed in our laboratory [35,57,58].

It is clear that PA 6-6 will undergo a more severe oxidative attack than PE, this attack being preferentially localized on C–H bonds in α position of nitrogen atoms. The chemical structures of the four main reactive species (i.e. reactive methylene, alkyl and peroxy radicals, and hydroperoxide) involved during aliphatic PAs oxidation are presented in Table 5.

At low to moderate temperature (typically below 200 °C), polymer oxidation is mainly initiated by the thermal decomposition of hydroperoxide groups [32]. In general, two distinct modes compete: unimolecular and bimolecular modes [35]:

Table 5
Chemical structure of the four main reactive species involved during thermal oxidation of aliphatic PAs.

Reactive specie	Notation	Chemical structure
Reactive methylene	PH	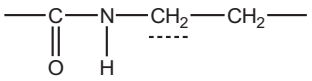
Alkyl radical	P$^{\bullet}$	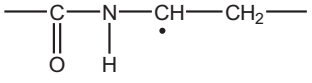
Peroxy radical	PO$_2^{\bullet}$	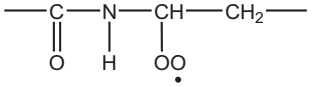
Hydroperoxide	POOH	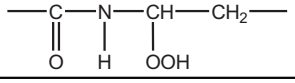

$$POOH \rightarrow PO^{\cdot} + {}^{\cdot}OH \qquad (k1u)$$

$$2POOH \rightarrow PO^{\cdot} + PO_2^{\cdot} + H_2O \qquad (k1b)$$

where k_{1u} and k_{1b} are the corresponding rate constants.

Hydroxyl and alkoxy radicals (HO• and PO•) are very reactive, their lifetime is too short to be observed by conventional spectroscopic techniques (for instance by ESR). Indeed, they are almost instantaneously transformed into P• radicals according to different competitive pathways.

PO• radicals can rearrange by β scission. In aliphatic PAs, it is suspected that this rearrangement involves preferentially the cleavage of C–N bonds because these latter present a much lower activation energy ($E_D \approx 292$ kJ mol^{-1}) than common C–C bonds ($E_D \approx 342$ kJ mol^{-1}). In this case, β scission reduces the substitution degree of amide groups by leading to the formation of amide and aldehyde chain-ends:

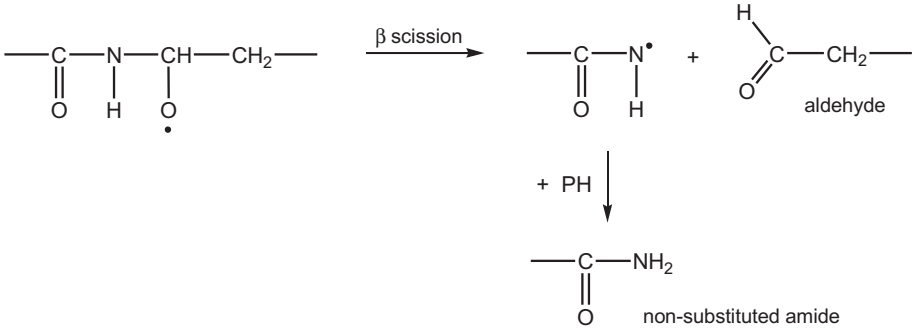

Of course, PO• radicals can also abstract labile hydrogens to polymer substrate. This reaction leads a very unstable hydroxylated amide group [11,28,39–42], of which the rapid decomposition leads also to amide and aldehyde chain-ends:

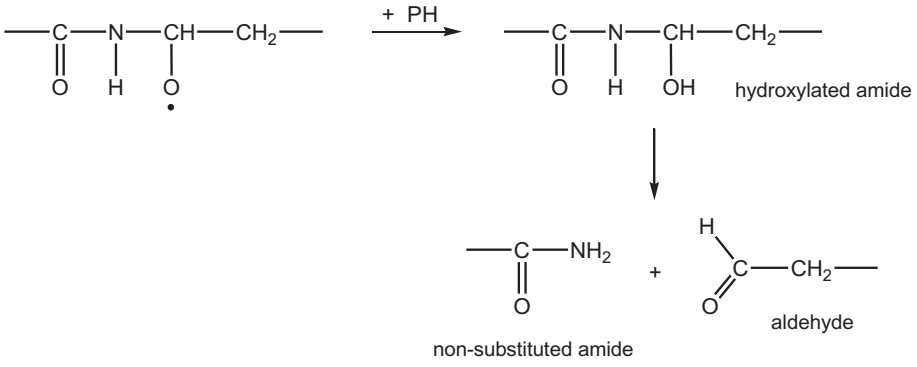

In contrast, HO• radicals will only abstract labile hydrogens to polymer substrate. As a result, unimolecular decomposition of hydroperoxides can be written as follows:

$$POOH \rightarrow PO^{\cdot} + {}^{\cdot}OH \qquad (k1u)$$

β scission $\quad PO^{\cdot} \rightarrow PNH_2 + PH = O + P^{\cdot} + S \quad [-PH, -CN]$

H abstraction $\quad PO^{\cdot} + PH \rightarrow PNH_2 + PH = O + P^{\cdot} + S \quad [-CN]$

H abstraction $\quad HO^{\cdot} + PH \rightarrow H_2O + P^{\cdot}$

Balance reaction : $POOH \rightarrow 2P^{\cdot} + PNH_2 + PH = O + H_2O + S \quad [-2PH, -CN] \qquad (k1u)$

where PNH_2, PH=O and S designate respectively amide and aldehyde chain-ends, and chain scissions.

As a same way, bimolecular decomposition can be written as follows:

$$2POOH \rightarrow PO^{\cdot} + PO_2^{\cdot} + H_2O \qquad (k1b)$$

β scission $\quad PO^{\cdot} \rightarrow PNH_2 + PH = O + P^{\cdot} + S \quad [-PH, -CN]$

H abstraction $\quad PO^{\cdot} + PH \rightarrow PNH_2 + PH = O + P^{\cdot} + S \quad [-CN]$

Balance reaction : $2POOH \rightarrow P^{\cdot} + PO_2^{\cdot} + PNH_2 + PH = O + H_2O + S \quad [-PH, -CN] \qquad (k1b)$

It is thus licit to write balance reactions for both decomposition modes because the cleavage of the O–O bond is largely slower than all other steps that follow. Let us notice that an important characteristic of these two balance reactions is that every initiation event leads to one chain scission (S), involving the cleavage of one C–N bond of amino-aliphatic type, and thus the formation of one aldehyde chain-end (PH=O). Such a high yield of chain scissions could explain the higher sensitivity of aliphatic PAs to embrittlement in an oxidizing environment, compared to common hydrocarbon polymers such as PP and PE.

Combinations of radical pairs will also lead to the formation of a large variety of oxidation products. First of all, secondary alkyl radicals can undergo coupling or disproportionation:

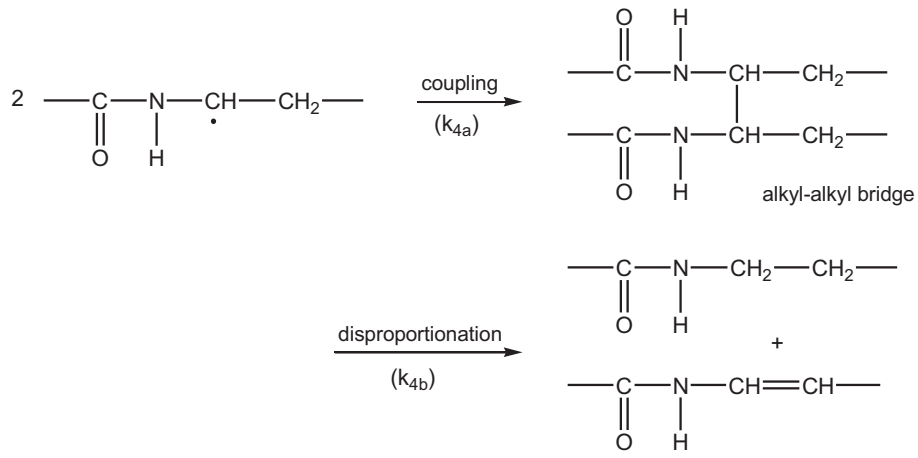

where k_{4a} and k_{4b} are the corresponding rate constants.

As a result, termination of alkyl radical pairs can be ascribed:

$$P^{\cdot} + P^{\cdot} \rightarrow {}_{\gamma 4}PP + (1-\gamma_4)PH + (1-\gamma_4)F + {}_{\gamma 4}X \; [-(1-\gamma_4)PH] \quad (k4)$$

$$\gamma_4 = \frac{k_{4a}}{k_4} \quad (11)$$

In a same way, termination between secondary alkyl and peroxy radicals can be ascribed:

$$P^{\cdot} + PO_2^{\cdot} \rightarrow \gamma_5 POOP + (1-\gamma_5)POOH + (1-\gamma_5)F + \gamma_5 X \quad [-(1-\gamma_5)PH] \quad (k5)$$

where F and X designate respectively double bonds and crosslink points. The global rate constant k_4 and the yield of alkyl–alkyl bridges γ_4 express as:

$$k_4 = k_{4a} + k_{4b} \quad (10)$$

where γ_5 is the yield of peroxide bridges.

In contrast, the case of secondary peroxy radicals is more complex. In principle, these latter would undergo coupling or disproportionation:

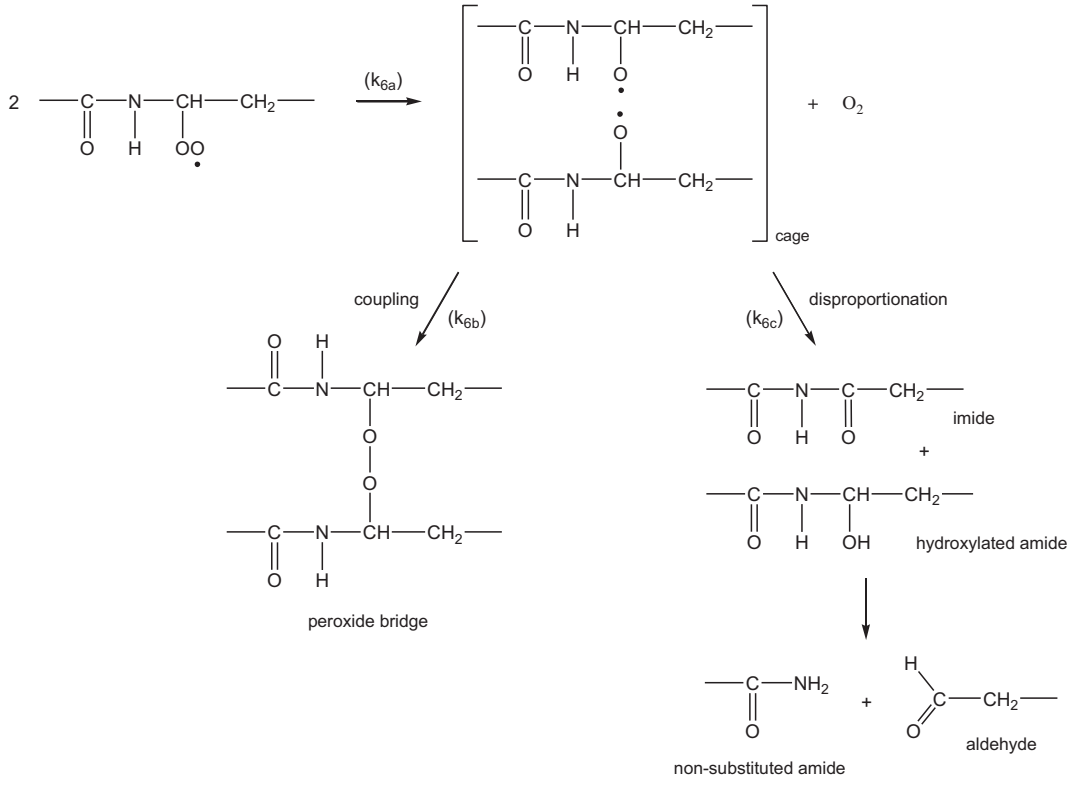

But, recent kinetic studies on PE oxidation have reached the conclusion that the termination of secondary peroxy radicals is not very efficient [59]. Indeed, a non-negligible part of alkoxy radical pairs can escape from the cage to initiate new radical oxidation chains. Finally, combination of secondary peroxy radical pairs can be ascribed:

$$PO_2^{\cdot} + PO_2^{\cdot} \rightarrow [PO^{\cdot}\,{}^{\cdot}OP]_{cage} + O_2 \quad \text{(k6a)}$$

$$[PO^{\cdot}\,{}^{\cdot}OP]_{cage} \rightarrow POOP + X \quad \text{(k6b)}$$

$$[PO^{\cdot}\,{}^{\cdot}OP]_{cage} \rightarrow NH(P=O)_2 + PNH_2 + PH=O + S \quad [-CN] \quad \text{(k6c)}$$

$$[PO^{\cdot}\,{}^{\cdot}OP]_{cage} \rightarrow 2P^{\cdot} + 2PNH_2 + 2PH=O + 2S \quad [-2PH, -2CN] \quad \text{(k6d)}$$

where $NH(P{=}O)_2$ designates imide groups.

Finally, a realistic mechanistic scheme for the thermal oxidation of PAs could be:

$$POOH \rightarrow 2P^{\cdot} + PNH_2 + PH=O + H_2O + S \quad [-2PH, -CN] \quad \text{(k1u)}$$

$$2POOH \rightarrow P^{\cdot} + PO_2^{\cdot} + PNH_2 + PH=O + H_2O + S \quad [-PH, -CN] \quad \text{(k1b)}$$

$$P^{\cdot} + O_2^{\cdot} \rightarrow PO_2^{\cdot} \quad \text{(k2)}$$

$$PO_2^{\cdot} + PH \rightarrow POOH + P^{\cdot} \quad \text{(k3)}$$

$$P^{\cdot} + P^{\cdot} \rightarrow \gamma_4 PP + (1-\gamma_4)PH + (1-\gamma_4)F + \gamma_4 X \quad [-(1-\gamma_4)PH] \quad \text{(k4)}$$

$$P^{\cdot} + PO_2^{\cdot} \rightarrow \gamma_5 POOP + (1-\gamma_5)POOH + (1-\gamma_5)F + \gamma_5 X \quad [-(1-\gamma_5)PH] \quad \text{(k5)}$$

$$PO_2^{\cdot} + PO_2^{\cdot} \rightarrow [PO^{\cdot}\,{}^{\cdot}OP]_{cage} + O_2 \quad \text{(k6a)}$$

$$[PO^{\cdot}\,{}^{\cdot}OP]_{cage} \rightarrow POOP + X \quad \text{(k6b)}$$

$$[PO^{\cdot}\,{}^{\cdot}OP]_{cage} \rightarrow NH(P=O)_2 + PNH_2 + PH=O + S \quad [-CN] \quad \text{(k6c)}$$

$$[PO^{\cdot}\,{}^{\cdot}OP]_{cage} \rightarrow 2P^{\cdot} + 2PNH_2 + 2PH=O + 2S \quad [-2PH, -2CN] \quad \text{(k6d)}$$

Let us notice that it is suspected that aldehyde groups rapidly oxidize into acid groups as already evidenced, for instance, in the case of saturated polyesters [57]. Such an assumption will be carefully checked from IRTF analysis.

3.2. Kinetic model

A kinetic model can be derived from the previous mechanistic scheme using the common theoretical concepts of chemical kinetics. It involves 5 non-linear differential equations:

$$\frac{d[POOH]}{dt} = -k_{1u}f_{PH}[POOH] - 2k_{1b}f_{PH}[POOH]^2 + k_3[PH][PO_2^{\bullet}] + (1-\gamma_5)k_5 f_{PH}[P^{\bullet}][PO_2^{\bullet}] \quad (12)$$

$$\frac{d[P^{\bullet}]}{dt} = 2k_{1u}f_{PH}[POOH] + k_{1b}f_{PH}[POOH]^2 - k_2[O_2][P^{\bullet}] + k_3[PH][PO_2^{\bullet}] - 2k_4[P^{\bullet}]^2 - k_5 f_{PH}[P^{\bullet}][PO_2^{\bullet}] + 2k_{6d}f_{PH}[PO^{\bullet\bullet}OP]_{cage} \quad (13)$$

$$\frac{d[PO_2^{\bullet}]}{dt} = k_{1b}f_{PH}[POOH]^2 + k_2[O_2][P^{\bullet}] - k_3[PH][PO_2^{\bullet}] - k_5 f_{PH}[P^{\bullet}][PO_2^{\bullet}] - 2k_{6a}[PO_2^{\bullet}]^2 \quad (14)$$

$$\frac{d[PO^{\bullet\bullet}OP]_{cage}}{dt} = k_{6a}[PO_2^{\bullet}]^2 - \left(k_{6b} + k_{6c} + k_{6d}f_{PH}\right)[PO^{\bullet\bullet}OP]_{cage} \quad (15)$$

$$\frac{d[PH]}{dt} = -2k_{1u}f_{PH}[POOH] - k_{1b}f_{PH}[POOH]^2 - k_3[PH][PO_2^{\bullet}] - (1-\gamma_5)k_5 f_{PH}[P^{\bullet}][PO_2^{\bullet}] - 2k_{6d}f_{PH}[PO^{\bullet\bullet}OP]_{cage} \quad (16)$$

where f_{PH} is a mathematical function introduced in the system of differential equations to avoid that the substrate concentration becomes negative at high conversion ratios of oxidation process. In a first approach, a hyperbolic mathematical form has been chosen to describe the changes of f_{PH} against [PH]:

$$f_{PH} = \frac{[PH]}{[PH] + \varepsilon} \quad (17)$$

with, typically: $\varepsilon = 10^{-2} << 1$. This function does not induce significant changes of the oxidation kinetics below a conversion value of about 99%.

This system of differential equations admits the following initial conditions (at $t = 0$):

$$[POOH] = [POOH]_0 = 5.0 \times 10^{-2} mol \cdot l^{-1}$$

$$[P^{\cdot}] = [PO_2^{\cdot}] = [PO^{\cdot}\,{}^{\cdot}OP]_{cage} = 0$$

and $[PH] = [PH]_0$

At this stage, it is important to recall that $[POOH]_0$ does not correspond to the real initial concentration of hydroperoxides within the material, but often to a higher value, since it takes into

accounts the presence of "extrinsic" species very difficult to titrate chemically (e.g. catalytic residues, polymer–oxygen complex, structural irregularities, etc.) which are also largely responsible for the earliest acts of polymer oxidation. However, since the decomposition rate of these latter vanishes rapidly with time of exposure, POOH decomposition becomes rapidly the main source of radicals.

The system of differential equations has been solved numerically using semi-implicit algorithms recommended for stiff problems of chemical kinetics, in particular the ODE23s solver of Matlab commercial software. Thus, it has given access to the changes against time of exposure of the main reactive species: [POOH], [$P^{\bullet}$], [$PO_2^{\bullet}$], [$PO^{\bullet}\ {}^{\bullet}OP]_{cage}$ and [PH] = $f(t)$.

These quantities have been used to calculate the changes of some important physico-chemical properties easily measurable experimentally and thus, chosen to check the validity of the kinetic model:

- Molecular changes:

$$\frac{d[O_2]_{abs}}{dt} = k_2[O_2][P^{\bullet}] - k_{6a}[PO_2^{\bullet}]^2 \tag{18}$$

$$\frac{d[PNH_2]}{dt} = k_{1u}f_{PH}[POOH] + k_{1b}f_{PH}[POOH]^2 + (k_{6c} + 2k_{6d}f_{PH})[PO^{\bullet\bullet}OP]_{cage} \tag{19}$$

$$\frac{d[PH = O]}{dt} = \frac{d[PNH_2]}{dt} \tag{20}$$

$$\frac{d[NH(P = O)_2]}{dt} = k_{6c}[PO^{\bullet\bullet}OP]_{cage} \tag{21}$$

$$\frac{d[C - N]}{dt} = -\frac{d[PNH_2]}{dt} \tag{22}$$

where $[O_2]_{abs}$ is the concentration of oxygen consumed by the chemical reaction with the polymer.

Thus, according to Eqs. (20) and (22), the changes in the concentration of amide (PNH_2) and aldehyde chain-ends (PH=O), and C–N bonds would be closely linked. The integration of these two equations leads to:

$$[PNH_2] = [PH = O] = [C - N]_0 - [C - N] \tag{23}$$

This important characteristic of the kinetic model will be carefully checked from IRTF analysis.

- Macromolecular changes:

$$\frac{dS}{dt} = \frac{d[PNH_2]}{dt} \tag{24}$$

$$\frac{dX}{dt} = \gamma_4 k_4[P^{\bullet}]^2 + \gamma_5 k_5 f_{PH}[P^{\bullet}][PO_2^{\bullet}] + k_{6b}[PO^{\bullet\bullet}OP]_{cage} \tag{25}$$

- And finally, the changes in molar masses, by using the classical Saito's equations [60,61]:

$$\frac{1}{M_n} - \frac{1}{M_{n0}} = S - X \tag{26}$$

$$\frac{1}{M_W} - \frac{1}{M_{W0}} = \frac{S}{2} - 2X \tag{27}$$

where M_{n0}, M_{W0}, M_n and M_W are respectively the number and weight average molar masses before and after thermal aging.

Let us notice that Eq (26) and (27) can be rewritten:

$$M_n = \frac{M_{n0}}{M_{n0}(S - X) + 1} \tag{28}$$

$$M_W = \frac{2M_{W0}}{M_{W0}(S - 4X) + 2} \tag{29}$$

4. Results and discussion

4.1. Simulation of molecular changes

The changes against time of exposure in the concentration of aldehyde chain-ends and broken C–N bonds in air between 90 and 160 °C are reported in Fig. 9.

As expected, in this temperature range, the oxidation induction time of additive free PA 6-6 is clearly too short to be correctly estimated. As a result, oxidation rate is maximum from the early periods of exposure, then decreases progressively with time. It vanishes at long term, presumably when the substrate concentration is totally depleted. Moreover, one can see that the cleavage of

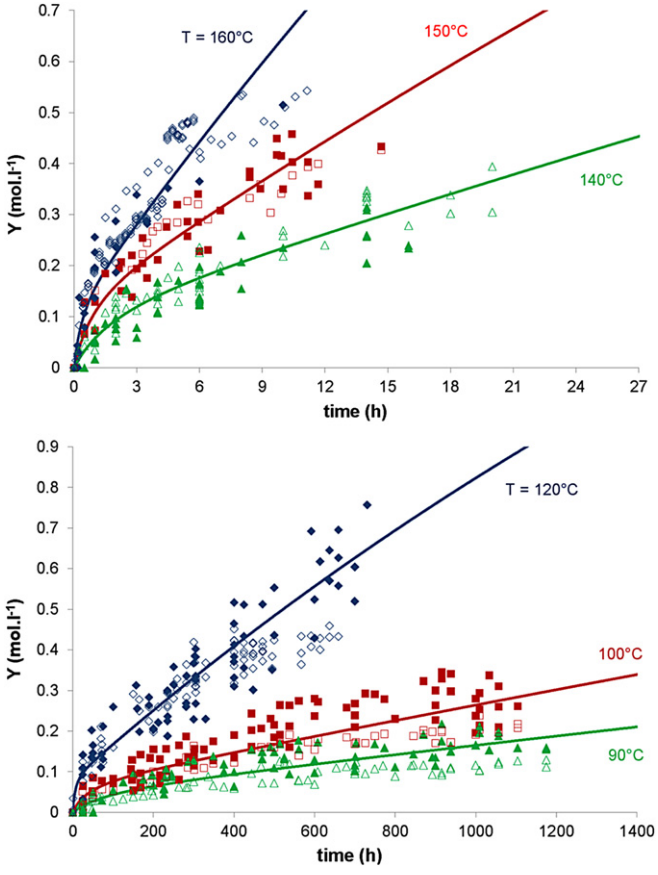

Fig. 9. Changes against time of exposure in the concentration of aldehyde chain-ends and broken C–N bonds in air between 90 and 160 °C. Comparison between theory (solid lines) and experiment (symbols). Concentrations of PH=O chain-ends and broken C–N bonds are represented by open and solid symbols respectively.

one C–N bond leads to the formation of one aldehyde chain-end, which confirms the validity of Eq. (23) and thus, constitutes of first proof in favor of the oxidation mechanistic scheme proposed for aliphatic PAs.

Eq. (20) (or Eq. (22)) has been used to tentatively simulate these experimental data. One can observe a satisfying agreement between theory and experiment in Fig. 9. Elementary rate constants have been determined between 90 and 160 °C by using the kinetic model as an inverse method. Their values are reported in Table 6. As an example, they are compared to the values determined for PE at 160 °C in previous studies made in our laboratory [32,33,35].

These values call for the following comments:

- Orders of magnitude of initiation and termination rate constants seem to be quite realistic. Indeed, they check the following hierarchy:

$$10^{12} > k_4 > k_5 > k_{6a} > k_{6d} \geq k_{6b} \approx k_{6c} >> 1 >> k_{1b} > k_{1u} \quad (30)$$

- As expected, POOH are more unstable in PA 6-6 than in PE. As an example, at 160 °C:

$$k_{1u}(\text{PA } 6-6) = 7.3 \times k_{1u}(\text{PE}) \text{ and } k_{1b}(\text{PA } 6-6) = 9.7 \times k_{1b}(\text{PE})$$

- As expected, $PO_2^{\bullet}$ radicals are more reactive in PA 6-6 than in PE. Indeed, let us recall that the apparent termination rate constant for the bimolecular termination of radicals can be written [33]:

$$k_{6app} = \frac{2k_{6a}k_t^2}{(k_t + k_{6d})(2k_t + k_{6d})} \quad (31)$$

with $k_t = k_{6b} + k_{6c}$.

Thus, at 160 °C:

$$k_{6\ app}(\text{PA } 6-6) = 6.6 \cdot 10^9 \text{l mol}^{-1}\ \text{s}^{-1} \text{ and } k_{6\ app}(\text{PE}) = 9.9 \cdot 10^8 \text{l mol}^{-1}\ s^{-1}$$

i.e. $k_{6\ app}$ (PA 6-6) ≈ 6.7 × $k_{6\ app}$ (PE)

- As expected, the bimolecular termination of $PO_2^{\bullet}$ radicals is not very efficient in PA 6-6, as previously found in PE. Indeed, about 85 and 70 mol% of alkoxy radical pairs escape from the cage to initiate new radical oxidation chains at 160 °C in PA 6-6 and PE respectively. This proportion decreases respectively to 38 and 19 mol% at 100 °C, but remains significant.

Table 7
Arrhenius parameters of elementary rate constants between 90 and 160 °C for aliphatic PAs. Comparison with the values obtained between 40 and 220 °C for PE in previous studies [32,33,35].

Polymer	PA 6-6		PE	
Arrhenius parameters	k_0	E_a (kJ mol^{-1})	k_0	E_a (kJ mol^{-1})
k_{1u} (s^{-1})	7.6 10^{12}	132	8.0 10^{12}	140
k_{1b} (l.mol^{-1} s^{-1})	1.4 10^9	94	2.8 10^9	105
k_2 (l.mol^{-1} s^{-1})	10^8	0	10^8	0
k_3 (l.mol^{-1} s^{-1})	1.8 10^9	63	1.5 10^{10}	73
k_4 (l.mol^{-1} s^{-1})	8.0 10^{11}	0	8.0 10^{11}	0
k_5 (l.mol^{-1} s^{-1})	5.0 10^{11}	0	2.3 10^{11}	0
k_{6a} (l.mol^{-1} s^{-1})	5.4 10^{16}	46	4.9 10^{19}	80
k_{6b} (s^{-1})	2.0 10^8	0	2.0 10^6	0
k_{6c} (s^{-1})	3.4 10^8	0	1.2 10^6	5
k_{6d} (s^{-1})	3.7 10^{13}	35	8.0 10^{12}	50

It was found that the elementary rate constants obey an Arrhenius law between 90 and 160 °C. Their Arrhenius parameters are reported in Table 7. They are compared to the values determined for PE in previous studies [32,33,35].

These values call for the following comments:

- Orders of magnitude of Arrhenius parameters of initiation and termination rate constants seem to be quite realistic. Indeed, they check the following hierarchies:

$$k_{1u0} >> k_{1b0} \text{ and } E_{1u} > E_{1b} \quad (32)$$

with typically:

$$k_{1u0} = 10^{12} - 10^{13} \text{l mol}^{-1}\text{s}^{-1} \text{ and } E_{1u} = 130 - 140 \text{ kJ mol}^{-1}$$

$$k_{1b0} = 10^9 - 10^{10} \text{l mol}^{-1}s^{-1} \text{ and } E_{1b} = 90 - 110 \text{ kJ mol}^{-1}$$

$$\text{And } k_{6d0} > k_{40} \approx k_{50} > k_{6c0} \approx k_{6b0} \quad E_{6d} > E_{6c} \geq E_{6b} \geq E_5 \approx E_4 \quad (33)$$

with typically:

$$k_{6d} = 10^{12} - 10^{13} \text{l mol}^{-1}\ \text{s}^{-1} \text{ and } E_{6d} = 30 - 50 \text{ kJ mol}^{-1}$$

Table 6
Values of elementary rate constants and yields used between 90 and 160 °C for the kinetic modeling of the thermal oxidation of aliphatic PAs. Comparison with the values obtained at 160 °C for PE in previous studies [32,33,35].

Polymer	PA 6-6						PE
T (°C)	90	100	120	140	150	160	160
k_{1u} (s^{-1})	8.0 × 10^{-7}	2.2 × 10^{-6}	1.8 × 10^{-5}	1.6 × 10^{-4}	4.0 × 10^{-4}	8.0 × 10^{-4}	1.1 × 10^{-4}
k_{1b} (l.mol^{-1}.s^{-1})	4.0 × 10^{-5}	9.0 × 10^{-5}	5.0 × 10^{-4}	1.7 × 10^{-3}	3.5 × 10^{-3}	6.0 × 10^{-3}	6.2 × 10^{-4}
k_2 (l.mol^{-1}.s^{-1})	10^8	10^8	10^8	10^8	10^8	10^8	10^8
k_3 (l.mol^{-1}.s^{-1})	1.6	2.7	7.7	19.6	30.3	45.8	23.8
k_4 (l.mol^{-1}.s^{-1})	8.0 × 10^{11}	8.0 10^{11}	8.0 10^{11}	8.0 10^{11}	8.0 10^{11}	8.0 10^{11}	8.0 10^{11}
k_5 (l.mol^{-1}.s^{-1})	5.0 × 10^{11}	5.0 × 10^{11}	5.0 × 10^{11}	5.0 × 10^{11}	5.0 × 10^{11}	5.0 × 10^{11}	2.3 × 10^{11}
k_{6a} (l.mol^{-1}.s^{-1})	8.0 × 10^9	2.6 × 10^{10}	6.0 × 10^{10}	5.0 × 10^{10}	9.5 × 10^{10}	1.6 × 10^{11}	1.1 × 10^{10}
k_{6b} (s^{-1})	2.0 × 10^8	2.0 × 10^8	2.0 × 10^8	2.0 × 10^8	2.0 × 10^8	2.0 × 10^8	2.0 × 10^6
k_{6c} (s^{-1})	3.4 × 10^8	3.4 × 10^8	3.4 × 10^8	3.4 × 10^8	3.4 × 10^8	3.4 × 10^8	3.0 × 10^5
k_{6d} (s^{-1})	3.2 × 10^8	4.7 × 10^8	7.9 × 10^8	1.2 × 10^9	1.8 × 10^9	2.2 × 10^9	7.5 × 10^6
γ_4 (%)	100	95	80	55	55	50	50
γ_5 (%)	100	95	80	55	55	50	50

$$k_{40} \approx k_{50} = 10^{11} - 10^{12} \text{l mol}^{-1}\ \text{s}^{-1} \text{ and } E_5 \approx E_4 = 0 \text{ kJ mol}^{-1}$$

$$k_{6c0} \approx k_{6b0} = 10^{6} - 10^{8} \text{l mol}^{-1}\ \text{s}^{-1},\ E_{6c} = 0 - 5 \text{ kJ mol}^{-1} \text{ and } E_{6b} = 0 \text{ kJ mol}^{-1}$$

- As expected, in both polymethylenic substrates, initiation is essentially initiated by the bimolecular decomposition of POOH. Indeed, let us recall that the critical POOH concentration for which initiation switches from unimolecular to bimolecular mode can be written [33]:

$$[\text{POOH}]_C = \frac{k_{1u}}{k_{1b}} = A\exp(-E_C/RT) \quad (34)$$

with $A = k_{1u0}/k_{1b0}$ and $E_C = E_{1u} - E_{1b}$.

It was found that $[\text{POOH}]_C$ is very close for PA 6-6 and PE:

$$[\text{POOH}]_C = 5.3 \cdot 10^3 \exp(-38000/RT) \quad \text{for PA 6 – 6}$$

$$[\text{POOH}]_C = 2.9 \cdot 10^3 \exp(-35000/RT) \quad \text{for PE}$$

As an example, at 160 °C:

$$[\text{POOH}]_C = 1.3 \cdot 10^{-1} \text{ moll}^{-1} \quad \text{for PA 6 – 6}$$

$$[\text{POOH}]_C = 1.7 \cdot 10^{-1} \text{moll}^{-1} \quad \text{for PE}$$

Such $[\text{POOH}]_C$ values are not so far from the initial hydroperoxide concentration: $[\text{POOH}]_0 = 5 \cdot 10^{-2}$ mol l^{-1}, used for kinetic modeling. Thus, at 160 °C, thermal oxidation starts in unimolecular mode, but switches rapidly into bimolecular mode. Since $E_{1u} > E_{1b}$ (typically, $E_C = 35–40$ kJ mol^{-1} for both polymethylenic substrates), $[\text{POOH}]_C$ is an increasing function of temperature. As a result, thermal oxidation is exclusively initiated by the bimolecular mode at low temperature (typically when $T < 70$ °C).

- Finally, the apparent termination rate constant $k_{6\ app}$ is almost temperature independent in the whole temperature range under study for PA 6-6, and above 120 °C for PE [33]. This characteristic of the oxidation kinetics of polymethylenic substrates will allow us to simplify the kinetic analysis on the temperature dependence of t_i and r_S.

4.2. Prediction of literature data

The kinetics curves of oxygen absorption in air between 100 and 200 °C have been computed from Eq. (18) for four aliphatic PAs: PA 6-6, PA 4-6, PA 6 and PA 12. In a first approach, it was assumed that the unique difference between all these polymers is the initial concentration of oxidizable CH groups in the amorphous phase (Table 2). Thus, calculations have been made by using the set of values of elementary rate constants and yields previously determined for PA 6-6 (Tables 6 and 7).

Then, the corresponding values of t_i and r_S have been determined graphically (as shown in Fig. 1). Since the values of t_i are very short for PAs (typically $t_i << 1$s), as previously observed experimentally by different authors [11,13–23,25–30], the kinetic analysis was only performed on values of r_S. These latter are reported in the Arrhenius diagram of Fig. 10. They are compared to the experimental values compiled from the literature for additive free aliphatic PAs [14–17,20,21,25,26,28], but also to the theoretical and experimental values reported for PE in previous studies [32,33].

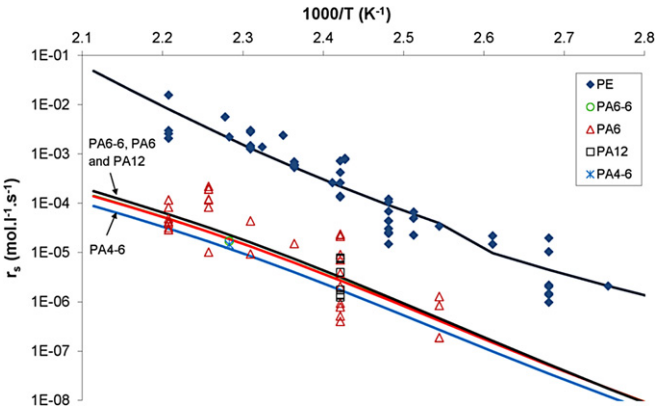

Fig. 10. Arrhenius plot of the maximal oxidation rate (r_S) of additive free aliphatic PAs and PE in air or pure oxygen (under atmospheric pressure) between 90 and 200 °C. Comparison between theory (solid lines) and experiment (symbols).

One can observe a satisfying agreement between theory and experiment for both types of polymethylenic substrates, which validates our general methodology for kinetic modeling. It appears thus possible to extend the oxidation mechanistic scheme, previously established for PE, to all types of polymethylenic substrates by adding elementary reactions specific to these latter. This study constitutes a first step towards the elaboration a non-empirical kinetic model for lifetime prediction of polymethylenic substrates.

The kinetic model confirms the universal character of the thermal oxidation kinetics of each polymethylenic substrate under study, but also allows to explain the main differences and similarities observed between the oxidation behaviors of these polymethylenic substrates:

- The fact that r_S takes almost the same value in all types of aliphatic PAs could be explained by the fact that the thermal oxidation kinetics is practically insensitive to small variations in substrate concentration.
- The fact that t_i and r_S take different values in aliphatic PAs and PE, could be explained by differences in stability of POOH groups, but also in reactivity of $PO_2^{\bullet}$ radicals.
- Finally, the fact that r_S presents almost the same activation energy E_S in both polymethylenic substrates can be explained by the fact that $k_{6\ app}$ is almost temperature independent. Indeed, in a first approach, orders of magnitude of E_S can be estimated from Eq. (2):

$$E_S = 2E_3 - E_{6\ app} \quad (35)$$

Since $E_{6\ app} \approx 0$, it comes:

$$E_S \approx 2E_3 \quad (36)$$

The numerical application of this last equation leads to:

$$E_S \approx 126 \text{ kJ} \cdot \text{mol}^{-1} \quad \text{for PA 6 – 6}$$

$$E_S \approx 146 \text{ kJgmol}^{-1} \quad \text{for PE}$$

These values are not so far from those determined experimentally (Table 1).

4.3. Prediction of macromolecular changes and embrittlement

The changes against time of exposure in the number average molar mass M_n in air between 90 and 160 °C are reported in Fig. 11.

One can see that M_n decreases catastrophically with time of exposure, which indicates that a predominant chain scission process takes place during the thermal oxidation of PA 6-6. As previously observed for the changes in the concentration of C–N bonds, the rate of chain scission is maximum from the early period of exposure, then decreases progressively with time.

Eq. (28) has been used to tentatively simulate these experimental data by using the set of values of elementary rate constants and yields determined previously (Tables 6 and 7). One can observe, here also, a satisfying agreement between theory and experiment, which constitutes a final proof in favor of the oxidation mechanistic scheme and kinetic model proposed for aliphatic PAs (Fig. 11).

At this stage of our investigations, the question is: How to predict the lifetime of PAs?

It has been shown that the non-empirical kinetic model, composed of Eq. (12)–(29), allows to simulate accurately both the molecular and macromolecular changes of PAs between 90 and 160 °C in air. This model can be also used to predict the oxidation kinetics of PAs at lower temperatures, since its elementary parameters (i.e. coefficient of oxygen solubility and rate constants) obey really an Arrhenius law (Tables 3 and 7). Thus, to predict the lifetime of PAs, one just needs to use a relevant structural endlife criterion. Such a criterion can be tentatively determined at both molecular and macromolecular scales.

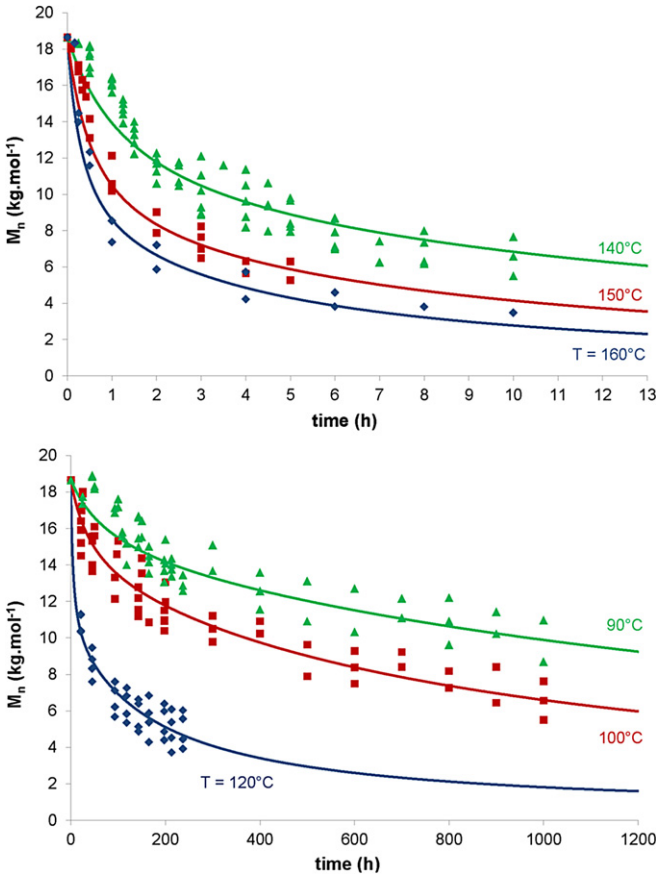

Fig. 11. Changes against time of exposure in the number average molar mass in air between 90 and 160 °C. Comparison between theory (solid lines) and experiment (symbols).

At first, let us recall that, in semi-crystalline polymers, the entanglement network allows the unwinding and drawing of chain segments located in the amorphous phase and connecting crystalline lamellae, i.e. plastic deformation. It is thus responsible for high values of tenacity and ultimate elongation. In contrast, in the absence of entanglement network, Van der Waals interactions are the only intermolecular forces. These latter are clearly too low to allow plastic deformation. In this case, the semi-crystalline polymer is extremely brittle (behaves like an eggshell) and is characterized by a value of tenacity about 2 or 3 decades lower than that for a ductile material [62].

Thus, in the case of a predominant chain scission process, one expects that the fracture properties of semi-crystalline polymers fall catastrophically when the entanglement network is deeply damaged, in particular when the number average molar mass reaches a critical value M_{nF} close to the entanglement threshold [63]:

$$M_{nF} \approx 5\ M_e \tag{37}$$

In a recent communication on PA 6-6 hydrolysis, an universal value of M_{nF} was proposed for aliphatic PAs [10]:

$$M_{nF} = 17 \pm 3\ \text{kg}\cdot\text{mol}^{-1}$$

It corresponds to a critical concentration of chain scissions:

$$S_F = \frac{1}{M_{nF}} - \frac{1}{M_{n0}} \tag{38}$$

i.e. $S_F = 5.6\times10^{-3}$ mol l^{-1}

This macromolecular endlife criterion seems to be also valid in the case of thermal oxidation of PA 6-6. Indeed, the ultimate elongation of PA 6-6 films, exposed in air between 90 and 160 °C or immersed in pure water between 60 and 90 °C, have been plotted versus their number average molar mass in Fig. 12. In both cases, one can see that the embrittlement of PA 6-6 occurs effectively for a M_{nF} value ranged between 18.6 and 16.5 kg mol^{-1}.

Now, let us recall that, in the case of thermal oxidation of PA 6-6, each chain scission event leads to the formation of one aldehyde chain-end. It is thus also possible to define a molecular endlife criterion:

$$[\text{PH} = \text{O}] = [\text{PH} = \text{O}]_F = 5.6\cdot10^{-3}\text{mol}\cdot\text{l}^{-1}$$

It corresponds to a conversion of only 0.06 mol% of the methylenic CH bonds, located in α position of nitrogen atoms, into aldehyde chain-ends.

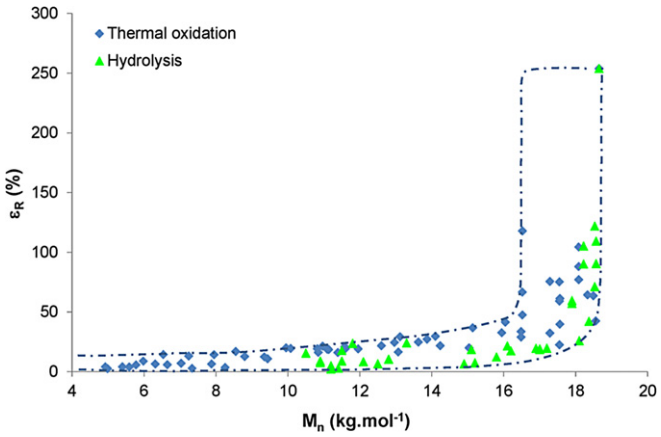

Fig. 12. Ultimate elongation versus number average molar mass for PA 6-6 films of about 100 μm thick exposed in air between 90 and 160 °C or immersed in pure water between 60 and 90 °C.

Unfortunately, such a molecular endlife criterion is out of reach of any common analytical techniques (e.g. FTIR or NMR).

5. Conclusions

A non-empirical kinetic model has been elaborated for describing the thermal oxidation not controlled by oxygen diffusion of additive free aliphatic PAs. This model has been derived from the oxidation mechanistic scheme previously established for PE, but improved by adding elementary reactions specific to PAs such as the rapid thermal decomposition of unstable hydroxylated amide groups. Its validity has been successfully checked from the changes in concentration of chemical groups and molar mass of PA 6-6 between 90 and 160 °C in air, but also from the temperature dependence of the maximal oxidation rate of PA 6-6, PA 6, PA 12 and PA 4-6 between 100 and 200 °C in air. Since its elementary parameters obey really an Arrhenius law, this model can be now used to predict the oxidation kinetics of aliphatic PAs at lower temperatures. It can be also used to predict lifetime by using a structural endlife criterion characterizing the ductile/brittle transition of aliphatic PAs. At this stage of our investigation, the most relevant criterion, which can be easily measurable experimentally (e.g. by rheometry in molten state or steric exclusion chromatography), is a critical value of molar mass: $M_{nF} \approx 17$ kg mol^{-1}.

This model confirms the universal character of the thermal oxidation kinetics of aliphatic PAs and PE whatever their origin, i.e. their initial molar mass, degree of branching, crystallinity ratio, concentration of impurities, structural irregularities, etc. It explains also the main differences and similarities between the oxidation behaviors of both polymethylenic substrates. At first, it was found that hydroperoxide groups are more unstable and peroxy radicals are more reactive in PAs than in PE. Such differences explain well why the thermal oxidation of methylene groups starts in the early periods of exposure for aliphatic PAs, whereas it starts after a well-marked induction period for PE. They explain also why, in contrast, the maximal oxidation rate is significantly lower (about 20–100 times lower) in aliphatic PAs than in PE. Moreover, it was found that the apparent termination rate constant of peroxy radical pairs is almost temperature independent in both polymethylenic substrates. This generality explains well why the maximal oxidation rate presents almost the same activation energy in both polymethylenic substrates.

The present study was a first attempt to extend the oxidation mechanistic scheme, previously established for PE, to other types of polymethylenic substrates by adding elementary reactions specific to these latter. The results obtained in the present study for aliphatic PAs are very promising. New challenges will be now to check the validity of this methodology on other types of linear polymethylenic substrates such as: aromatic PAs and saturated polyesters (e.g. PET and PBT), but also on tridimensional polymethylenic substrates such as: styrene crosslinked unsaturated polyesters, diamine and anhydride crosslinked polyepoxys, etc.

References

[1] Atofina technical report. Thermoplastic polymers for off-shore flexible pipes. Atofina Technical Polymers Division; February 2002.
[2] Meyer A, Jones N, Lin Y, Kranbuelh D. Characterizing and modelling the hydrolysis of polyamide 11 in a pH 7 water environment. Macomolecules 2002;35:2784–98.
[3] Jacques B, Werth M, Merdas I, Thominette F, Verdu J. Hydrolytic ageings of polyamide 11 – hydrolysis kinetics in water. Polymer 2002;43:6439–47.
[4] Merdas I, Thominette F, Verdu J. Hydrolytic ageings of polyamide 11 – effect of carbon dioxide on polyamide 11 hydrolysis. Polym Degrad Stab 2003;79: 419–25.
[5] Cribbs D, Ogale AA. Hydrolytic degradation of nylon 6-6 pile carpet fibers. Textile Res J 2003;73(2):98–104.
[6] Romao W, Castro EVR, Filho EAS, Guimaraes RCL, Silva ANL, Teixeira SCS, et al. Aging of polyamide 11 used in the manufacture of flexible piping. J Appl Polym Sci 2009;114:1777–83.
[7] Alam TM. Solution ^{17}O NMR study of thermal hydrolysis in nylon 6-6. Polymer 2003;44:6531–6.
[8] Bernstein R, Derzon DK, Gillen KT. Nylon 6-6 accelerated aging studies: thermal-oxidative degradation and its interaction with hydrolysis. Polym Degrad Stab 2000;67:69–78.
[9] Bernstein R, Gillen KT. Nylon 6.6 accelerating aging studies: II. Long-term thermal-oxidative and hydrolysis results. Polym Degrad Stab 2010;95: 1471–9.
[10] El Mazry C, Correc O, Colin X. A new kinetic model for predicting PA 6-6 hydrolysis and its mechanical embrittlement. Polym Degrad Stab 2012;97: 1049–59.
[11] Karstens T, Rossbach V. Thermo-oxidative degradation of polyamide 6 and 6-6. Kinetics of the formation and inhibition of UV/Vis-active chromophores. Makromol Chem 1989;190:3033–53.
[12] Karstens T, Rossbach V. Thermo-oxidative degradation of polyamide 6 and 6-6. Structure of UV/Vis-active chromophores. Makromol Chem 1990;191:757–71.
[13] Tcharkhtchi A. Chemiluminescence of polyepoxys and polyamides, PhD Thesis, ENSAM, Paris, France; 1993.
[14] Lanska B. Stabilization of polyamides. I. The efficiency of antioxidants in polyamide 6. Polym Degrad Stab 1996;53:89–98.
[15] Lanska B, Matisova-Rychla L, Brozek J, Rychly J. Chemiluminescence of polyamides. II. Luminescence accompanying thermooxidation of lactam-based polyamides related to the content of end-groups of molecules. Polym Degrad Stab 1999;66:433–44.
[16] Lanska B, Doskocilova D, Matisova-Rychla L, Puffr R, Rychly J. Thermooxidation of lactam-based polyamides with amino end-groups. Thermooxidation of hexane-6-lactam and decomposition of 6-hydroperoxyhexano-6-lactam in the presence of primary amines. Polym Degrad Stab 1999;63:469–79.
[17] Frosstrom D, Terselius B. Thermo-oxidative stability of polyamide 6 films. I. Mechanical and chemicals characterisation. Polym Degrad Stab 2000;67:69–78.
[18] Frosstrom D, Reitberger T, Terselius B. Thermo-oxidative stability of polyamide 6 films. II. Chemiluminescence techniques. Polym Degrad Stab 2000; 67:255–61.
[19] Frosstrom D, Svensson L-G, Terselius B. Thermo-oxidative stability of polyamide 6 films. III. Isothermal microcalorimetry. Polym Degrad Stab 2000;67: 263–9.
[20] Lanska B, Matisova-Rychla L, Rychly J. Chemiluminescence of polyamides. III. Luminescence accompanying thermooxidation of lactam-based polyamides stabilized by antioxidants. Polym Degrad Stab 2001;72:249–58.
[21] Lanska B, Matisova-Rychla L, Rychly J. Stabilization of polyamides. V. Thermooxidation of hexane-6-lactam in the presence of copper salts. Polym Degrad Stab 2005;89:534–44.
[22] Grigg M.N. Thermo-oxidative degradation of polyamide 6, PhD Thesis, Queensland University of Technology, Australia; 2006.
[23] Shu Y, Ye L, Yang T. Study on the long-term thermal-oxidative aging behavior of polyamide 6. J Appl Polym Sci 2008;110:945–57.
[24] Kiliaris P, Papasrydes CD, Pfaendner R. Influence of accelerated aging on clay-reinforced polyamide 6. Polym Degrad Stab 2009;94:389–96.
[25] Dong W, Gijsman P. Influence of temperature on the thermo-oxidative degradation of polyamide 6 films. Polym Degrad Stab 2010;95(6):1054–62.
[26] George GA. An oxyluminescence investigation of the auto-oxidation of nylon 6-6. Polym Degrad Stab 1979;1(3):217–36.
[27] Allen NS, Harrison MJ, Follows GW, Matthews V. Thermal and photo-chemical degradation of nylon 6-6 polymer: Part I. Influence of amine-carboxyl end group balance on luminescent species. Polym Degrad Stab 1987;19:77–95.
[28] Gijsman P, Tummers D, Janssen K. Differences and similarities in the thermooxidative degradation of polyamide 4-6 and 6-6. Polym Degrad Stab 1995; 49:121–5.
[29] Cerruti P, Carfagna C, Rychly J, Matisova-Rychla L. Chemiluminescence from oxidation of polyamide 6-6. I. The oxidation of pure polyamide. Polym Degrad Stab 2003;82:477–85.
[30] Lanska B, Matisova-Rychla L, Rychly J. Chemiluminescence accompanying autoxidation of lactams and thermolysis of lactam hydroperoxides. Polym Degrad Stab 1998;61:119–27.
[31] Colin X, Fayolle B, Audouin L, Verdu J. The classical kinetic model for radical chain oxidation of hydrocarbon substrates initiated by bimolecular hydroperoxide decomposition. Int J Chem Kin 2006;38(11):666–76.
[32] Colin X, Fayolle B, Audouin L, Verdu J. About a quasi-universal character of unstabilised polyethylene thermal oxidation kinetics. Polym Degrad Stab 2003;80(1):67–74.
[33] Khelidj N, Colin X, Audouin L, Verdu J, Monchy-Leroy C, Prunier V. Oxidation of polyethylene under irradiation at low temperature and low dose rate. Part II-Low temperature thermal oxidation. Polym Degrad Stab 2006;91(7):1598–605.
[34] Audouin L, Achimsky L, Verdu J. Modelling of hydrocarbon polymer oxidation. In: Halim Hamid S, editor. Handbook of polymer degradation. 2nd ed. New-York: Marcel Dekker; 2000. p. 727–63. Chap. 20.
[35] Colin X, Audouin L, Verdu J. Determination of thermal oxidation rate constants by an inverse method. Application to polyethylene. Polym Degrad Stab 2004; 86:309–21.
[36] Van Krevelen DW, Te Nijenhuis K. Physical properties of most important polymers. In: Property of polymers. 4th ed. Amsterdam, The Netherlands: Elsevier; 2009. p. 928–9. Tab. V.

[37] Mark JE. Polymer data handbook. 2nd ed. New York: Oxford University Press; 1999.
[38] Colin X, Audouin L, Verdu J, Rozental-Evesque M, Rabaud B, Martin F, et al. Aging of polyethylene pipes transporting drinking water disinfected by chlorine dioxide. I-Chemical aspects. Polym Eng Sci 2009;49(7):1429–37.
[39] Sagar BF. Autoxidation of N-alkyl-amides. Part II. A-alkyl-amide hydroperoxides and di-N-alkyl-amide peroxides. J Chem Soc B 1967;428-439.
[40] Tang L, Sallet D, Lemaire J. Photochemistry of polyundecamides. I. Mechanisms of photooxidation at short and long wavelengths. Macromolecules 1982;15(5):1432–7.
[41] Roger A, Sallet D, Lemaire J. Photochemistry of aliphatic polyamides. IV. Mechanisms of photooxidation of polyamides 6, 11 and 12 at long wavelengths. Macromolecules 1986;19(3):579–84.
[42] Gonçalves ES, Poulsen L, Ogilby PR. Mechanism of the temperature dependent degradation of polyamide 6-6 films exposed to water. Polym Degrad Stab 2007;92(11):1977–85.
[43] Felder RM, Huvard GS. Permeation, diffusion and sorption of gases and vapors. In: Fava RA, editor. Methods of experimental physics: polymers. New York: Academic Press; 1980. p. 315–77.
[44] ASTM F1307-02. Standard test method for oxygen transmission rate trough dry packages unsing a coulometric sensor; 2007.
[45] ISO 15105-2. Plastics – film and sheeting – determination of gas-transmission rate – part 2: equal-pressure method; 2003.
[46] Crank J. Diffusion in polymers. London: Academic Press; 1975.
[47] Mark JE. Polymer data handbook. 2nd ed. New York: Oxford University Press; 2009.
[48] Van Krevelen DW, Te Nijenhuis K. Property of polymers. 4th ed. Amsterdam, The Netherlands: Elsevier; 2009.
[49] Barrer RM. Permeation, diffusion and solution of gases in organic polymers. Trans Faraday Soc 1939;35:628–43.
[50] Van Krevelen DW, Te Nijenhuis K. Properties determining mass transfer in polymeric systems. In: Property of polymers. 4th ed. Amsterdam, The Netherlands: Elsevier; 2009. p. 660. Chap. 18.
[51] Celina M, Gillen KT. Oxygen permeability measurements on elastomers at temperatures up to 225 °C. Polymer 2005;38:2754–63.
[52] Cannon CG. The infrared spectra and molecular configurations of polyamides. Spectrochim Acta 1960;16(3):302–19.
[53] Bueche F. Viscosity, self-diffusion and allied effects in solid polymers. J Chem Phys 1952;20(12):1959–64.
[54] Bueche F. The viscoelastic properties of plastics. J Chem Phys 1954;22(4): 603–9.
[55] Kamiya Y, Niki E. In: Jellinek HHG, editor. Aspect of degradation and stabilisation of polymers. New York: Elsevier; 1978. p. 86 [Chapter 3].
[56] Korcek S, Chenier JHB, Howard JA, Ingold KU. Absolute rate constants for hydrocarbon autoxidation. XXI. Activation energies for propagation and the correlation of propagation arte constants with carbon-hydrogen bond strengths. Can J Chem 1972;50(14):2285–97.
[57] Nait-Ali LK, Colin X, Bergeret A. Kinetic analysis and modeling of PET macromolecular changes during its mechanical recycling by extrusion. Polym Degrad Stab 2011;96(2):236–46.
[58] Coquillat M, Verdu J, Colin X, Audouin L, Nevière R. Thermal oxidation of polybutadiene. Part II-Mechanistic and kinetic schemes for additive free uncrosslinked polybutadiene. Polym Degrad Stab 2007;92(7):1334–42.
[59] Khelidj N, Colin X, Audouin L, Verdu J, Monchy-Leroy C, Prunier V. Oxidation of polyethylene under irradiation at low temperature and low dose rate. Part I- the case of "pure" radiochemical initiation. Polym Degrad Stab 2006;91(7):1593–7.
[60] Saito O. On the effects of high energy radiation to polymers. I. Crosslinking and degradation. J Phys Soc Jpn 1958;13(2):198–206.
[61] Saito O. On the effects of high energy radiation to polymers. II. End-linking and gel fraction. J Phys Soc Jpn 1958;13(12):1451–64.
[62] Fayolle B, Richaud E, Colin X, Verdu J. Review: degradation-induced embrittlement in semi-crystalline polymers having their amorphous phase in rubbery state. J Mater Sci 2008;43:6999–7012.
[63] Kausch HH, Heymans N, Plummer CJ, Decroly P. Matériaux polymères. Propriétés Mécaniques et Physiques. Principes de Mise en Œuvre. Lausanne: Presses Polytechniques et Universitaires Romandes; 2001. p. 249.